PCCP

Accepted Manuscript

ROYAL SOCIETY OF CHEMISTRY

www.rsc.org/pccp

Theoretical investigation on structural and electronic properties of organic dye C258 on TiO_2 (101) surface in dye sensitized solar cells

Ping-Ping Sun, Quan-Song Li,* Li-Na Yang, Zhu-Zhu Sun, Ze-Sheng Li *

Key Laboratory of Cluster Science of Ministry of Education, Beijing Key Laboratory of Photoelectronic/Electrophotonic Conversion Materials, Beijing Key Laboratory for Chemical Power Source and Green Catalysis, School of Chemistry, Beijing Institute of Technology, Beijing 100081, China

* Corresponding author at: 5 South Zhongguancun Street Haidian Zone, Beijing 10081, China. Tel.: +86 10 68918670; fax: +86 10 68918670

E-mail: liquansong@bit.edu.cn; zeshengli@bit.edu.cn.

ABSTRACT: The structural and electronic properties of an organic dye C258 before and after adsorbed onto the TiO_2 (101) surface with two adsorption modes, monodentate (Mha) and bidentate bridging (BBH), have been investigated in detail. The combination of density functional tight binding (DFTB), density functional theory (DFT), and time-dependent DFT (TDDFT) approaches are employed. DFT calculations show that C258 has remarkable charge-transfer characteristics, which favors fast electron injection from the excited dye to the conduction band of TiO_2. A detailed analysis of the adsorbate contributions of the dye molecule to band states of TiO_2 shows strong coupling of adsorbate orbitals with the substrate orbitals. Significant electronic transfer characteristic across the interface reveals direct electron injection mechanism arising from the electronic excitation from the anchoring group of C258 to the conduction bands of TiO_2. The adsorption energy and the electron density distribution demonstrate that the BBH structure is more stable and has a stronger coupling with TiO_2 than the Mha pattern, which can better promote the electron injection to increase the efficiency of dye-sensitized solar cells (DSSCs).

Keywords: dye-sensitized solar cell, adsorption mode, density of states, electron injection

1. Introduction

Since people are challenging for global energetic and environmental crisis with the rapid development of population and economy, renewable energy sources based on eco-friendly alternative solar sources have caused more and more attention. Dye sensitized solar cells (DSSCs) are considered as one of the most promising photovoltaic devices due to their low costs, ease of manufacture, and relatively high conversion efficiency.[1-4] In order to increase both the efficiency of light-harvesting and photoexcited electron transfer, great efforts have been made in search of proper dyes as sensitizers.[3-14] Dyes based on ruthenium polypyridyl complexes, such as N3 and N719, have been reported with impressive solar to electric power efficiency over 11%.[3, 5, 6] Zn-metalated porphyrin YD2-o-C8 in conjunction with cobalt (II/III)-based redox electrolyte reached a high record of 12.3% in 2011.[7] In 2014，a molecularly engineered porphyrin dye, coded SM315, refreshed the record with 13% efficiency.[12] Comparing with typical metal complex dyes, metal-free organic dyes have a rapid development in recent years, owing to their high molar extinction coefficient, tunable structures, low-cost and environmental friendly compatibility for large scale applications with relatively high efficiency up to 11.5-12.8%.[10]

Among the metal free organic dyes, triphenylamine (TPA)-based dyes, such as C217, C257, C258, C259, have been extensively investigated, because TPA group has the excellent electron donating and transporting capability, and its particular structure can prevent dye aggregation and constrain cationic charge from the semiconductor surface and therefore efficiently reduce the charge recombination.[10, 15-19] The

TPA-based dyes show a typical donor-π-acceptor (D-π-A) structure with TPA part as the electron donor and benzoic acid (BA) part as the acceptor. It is well known that both the dye structures and electron density distributions of frontier orbitals in the dyes adsorbed onto TiO_2 played important roles in electron injection and charge recombination processes.[20, 21]

In addition to the nature of the dye itself, the combination pattern of dye and TiO_2 also strongly affect the electron transfer processes (electron injection and recombination) and further influence the efficiency of DSSCs, so it has received widespread attention from both experimental and theoretical viewpoints.

By analogy with other metal-oxide surfaces, such as rutile, several different geometries of dye on anatase (101) can be figured out. Molecular and dissociative adsorptions of formic acid are the two most studied types of configurations. In case of molecular coordination, there are four different binding forms, which are monodentate through CO (Mha), monodentate through OH (Mhb), bidentate chelating (B(h)), and bidentate bridging (BB(h)).[22] For dissociative adsorption, there are also four possible patterns, monodentate ester-type (MH), monodentate bidentate chelating (MBC), bidentate chelating (BH), and bidentatte bridging (BBH).[22] A series of studies show that Mha and BBH are the most stable adsorption for molecular and dissociative adsorption, respectively.[22-28] However, opinions are divided as for the stability of the two patterns. Vittadini *et al*. found that adsorbing different molecules will produce different stability through analyzing the adsorption energy of the different adsorption modes.[22] Some studies suggest that Mha is the most stable arrangement about the

adsorption of formic acid on anatase (101) surface. Besides, Sodeyama *et al*. compared various binding function protonated and deprotonated adsorption with one and two anchors in both Mha and BBH configurations for black dye N749 adsorbed onto TiO_2 (101), and their calculation showed that protonated adsorption with one anchor in Mha mode was the most stable structure.[29] Whereas, other studies predict BBH more stable than Mha.[30, 31] A combined experimental and computational investigation of anthracene based sensitizers revealed that BBH was the most favorable configuration for M1 and M3 dyes.[23] Grinter *et al*. used anharmonic vibrational spectra to investigate the adsorption mode of acetic acid on anatase TiO_2 (101),[27] and so did Matthew's work with the same system as Grinter' also proved Srinivas's opinion.[28] O'Rourke with his partners made a comparison of Mha and BBH for C2-1 dye showed that BBH was favored over 0.37 eV than Mha.[24] While for the system with two anchoring groups, Schiffmann *et al*. believed that a mixed bidentate/monodentate binding in the presence of protons is the favorable binding function for ruthenium bipyridyl dyes N3, N719 and N712.[32] Nevertheless, Labat and his co-workers considered that a mixed bidentate/monodentate biding presented similar adsorption energy to bidentate/bidentate binding for N3 dye, and both modes are outlining the flexibility of N3 for binding to the TiO_2 surface.[33] Integrated the above opinions, the adsorption modes arising from the strong bonding interactions between C258 and the surface of TiO_2 are limited to Mha and BBH patterns, depending on the number of oxygens used by the molecule/anion to coordinate with the surface Ti_{5c} sites.[22]

Both cluster models[34-36] and periodic models[33, 37-39] have been widely used in theoretical studies on adsorption modes and electronic properties. However, the cluster models are usually too small to describe the real morphology and properties of materials and not as convincing as periodic models. Fortunately, the density functional tight binding (DFTB) approach has been shown to provide results of DFT quality for the structural, electronic and optical properties of large molecules in clusters as well as periodic solids with high efficiency and good agreement with results obtained by DFT calculations and in experiments.[40-49]

In this work, considering the Mha and BBH adsorption patterns, we systematically explored the structural and electronic properties of an emblematic TPA dye C258 before and after adsorption on TiO_2 (101) surface by performing DFT and DFTB calculations. The inherent nature of the periodical system about the strength of the coupling degree and the mechanism of electron injection are also discussed.

2. Computational details

The calculations on the structure and electronic properties of the pure dye in the present work have been performed with Gaussian09 program.[50] The ground-state geometric optimization was carried out by the hybrid functional B3LYP coupled with the 6-31G* basis set in tetrahydrofuran (THF) solution (the dielectric constant ε =7.6).[51] Frequency calculation was then carried out to confirm the nature of obtained minima at the same theory level as geometry optimizations. The adsorption spectrum was calculated by TDDFT method using MPW1K hybrid density functional[52] with 6-31G* basis set in THF solution. In DFT and TDDFT calculations, the solvation

effects were simulated by a conducting polarizable continuum model (C-PCM).[53]

The structures and properties of C258 adsorbed on TiO_2 (101) surface were studied by using self-consistent charge density functional tight binding (SCC-DFTB) method. DFTB is an approximation to DFT based on a second-order expansion of DFT total energy around a reference electron density with significantly reduced computational cost. We used a periodically repeated slab geometry appropriately cutting from the most stable anatase TiO_2 (101) surface,[54, 55] where the (101) TiO_2 surface was constructed from a 8×8 monocline surface slab, corresponding to 12 atomic layers containing 256 titanium and 512 oxygen atoms, with a vacuum ~ 60 Å wide in the *z* direction. For the sampling of the Brillouin zone, the Monkhorst-Pack grid parameters (4×4×1) were employed for TiO_2 anatase (101) surface, keeping the supercell volume fixed with lattice vectors a = 43.5 Å, b = 30.21 Å, c = 65.8 Å, α= 90 °, β= 90 °, γ= 110.3 °. The outmost atoms of TiO_2 anatase (101) surface are 2-fold (O_{2C}) and 3-fold (O_{3C}) coordinated oxygen as well as 5-fold (Ti_{5C}) and 6-fold (Ti_{6C}) coordinated titanium. The unsaturated O_{2c} and Ti_{5c} atoms tend to tighten their bonds with the adsorbed molecules and relax inward. On the contrary, saturated O_{3c} and Ti_{6c} atoms relax outwards. In all calculations, the dye molecule was adsorbed on the upper surface of the slab only, since the coordinatively unsaturated O_{2C} and Ti_{5C} atoms on the surface tend to tighten their bonds with the nearest neighbors.

For the $(TiO_2)_{256}$ and C258/$(TiO_2)_{256}$ periodic systems with hundreds of atoms, we take advantage of the efficiency of DFTB method available in the DFTB+ code[56] for geometry optimization, structure and electronic properties analysis, and using periodic

boundary conditions (PBCs). In DFTB calculations, the full geometric optimization was performed by using the conjugate gradient algorithm until the residual forces were below 5×10^{-4} au and the charge convergence criterion to 10^{-5} electrons. All precomputed matrix elements are held in Slater-Koster files, downloaded from http://www.dftb.org. The basis sets of numerically described *s*, *p*, *d* atomic orbitals for S and Ti, *s*, *p* orbitals for C, N, O, and *s* orbital for H. The mio-1-1 parameter set was used for O, C, N, S interactions[57] and the tiorg-0-1 parameter set for Ti interactions[58] in all calculations.

Adsorption energy refers to the energy change of anatase system giving rise to the adsorption of dye molecule on the TiO_2 surface, and can be calculated by the following Eq. (1)[59]:

$$E_{ads} = E(\text{dye}) + E(TiO_2) - E(\text{dye}/TiO_2) \quad (1)$$

where, E (dye), E (TiO_2) and E (dye/ TiO_2) are the energies of the isolated dye molecule, the relaxed bare TiO_2, and the adsorption system, respectively. With this definition, a positive E_{ads} value corresponds to the stable adsorption on the surface.

In DFTB calculations, the solvation effects were not considered because no solvation models are available in the present DFTB code.

To validate the reliability of DFTB parameters, test calculations were performed on C258 molecule and $(TiO_2)_{36}$ periodical model in vacuum. For the structure of ground-state C258, our DFTB results about C=O, C-N bond length of 1.220 Å and 1.399 Å, bond angle C-N-C of 121.1 ° are in good agreement with DFT values of 1.219 Å, 1.404 Å and 121.1 °, respectively. In terms of energy, the calculated band gap

by DFTB of $(TiO_2)_{36}$ (2.856 eV) is close to GGA-PBE result (3.02 eV) and experimental value (3.2 eV). The above tests indicate that the accuracy of the Slater-Koster parameters used for DFTB is comparable with DFT calculations to study C258 and TiO_2 nanostructures.

3. Results and discussions

3.1 Structural and electronic properties of free dyes

The dyes play an important role in light absorption and charge injection from photo-excited state to conduction band of semiconductor, which are key factors in terms of conversion efficiency for solar cell. In this work, we focus on dye C258, where TPA acting as electron donor and BA unit as electron acceptor, with a high power conversion efficiency (PCE) over 10% reported by Wang's group.[10] The optimized geometry of C258 is displayed in Fig. 1. For C258, the π linker is a cyclopentadithiophene (CPDT) connected to TPA group and conjugated with benzothiadiazole (BT) unit. In addition, there is good coplanarity between the bridging unit and anchoring group excluding the branched chains, which is beneficial for the electron transfer.

To probe into the electronic property of C258, its frontier orbitals of the highest occupied molecular orbital (HOMO) and the lowest unoccupied molecular orbital (LUMO) are depicted in Fig. 1. The frontier orbitals are highly delocalized, which is a typical feature of D-π-A system. The HOMO is mainly populated over the substituted TPA and adjacent π linker units, thus the delocalization of π-electrons of the donor group can enhance the conjugation between the donor unit and the π conjugation

segment and extend the effective conjugation length for the molecular skeleton, which can increase the π-π* transition probability of the charge transfer, resulting in a high adsorption coefficient and improved light harvesting capacity. While the LUMO is mainly distributed over the π linker and the acceptor BA group, especially over the BT unit. This spatial arrangement of HOMO and LUMO are an ideal condition for DSSCs. During photo-excitation, electron is transferred from the TPA unit through the π bridge to the benzoic acid, which promotes strong coupling of the excited state wave function with the Ti (3*d*, t_{2g}) orbitals and subsequently facilitates the electron injection to the TiO_2 conduction bands. Furthermore, such photo-excitation features may slow down the recombination of the electrons injected in TiO_2 with the oxidized dye molecules.[19]

In the computed adsorption spectrum of C258, as Fig. 2 shows, the simulated maximum absorption appears in the visible region of 559 nm (*f*= 1.4287), which agrees well with the experimental value of 545 nm.[10] The maximum absorption is dominated by HOMO to LUMO transition with a proportion over 80%. In most cases, the transition from HOMO to LUMO is the most important contribution to the excitation from the ground state (S_0) to the lowest excited state (S_1), which usually corresponds to the maximum absorbance of organic dyes.[9] For C258, the transition from HOMO to LUMO has a high proportion of nearly 80% in the construction of the S_0-S_1 excitation. A broad absorption is necessary to obtain good overlap with the solar spectrum to produce a large photocurrent response. And it is probably one of the key reasons why C258 displays a high PCE in DSSCs.[10]

The difference in electron density distribution between HOMO and LUMO results in the intramolecular charge separation between the acceptor and the donor of sensitizer upon excitation, indicating that large dipole moment may exist in the S_1 state compared to the S_0 state.[60] To explore the charge-transfer features of these electronic transitions, we examined the variation of the total electron density between the S_0 and S_1 states. The corresponding electron density difference map is incorporated into Fig. 2, where the purple and red regions refer to an increase and a decrease of electron density, respectively. As the density difference map reveals, there are remarkable charge-transfer characteristics for these transitions, in which the electron density in the photoexcited dye C258 exhibits a decrease at the TPA group and an increase at the CPDT group and the benzoic acid anchor, indicating that the TPA moiety and the π-bridge CPDT moieties act as the electron-donating and electron-withdrawing groups, respectively. Accordingly, a high electron density at the anchoring group of the photoexcited C258 dye will make the electron injection from the excited dye to the conduction band of TiO_2 more effectively, resulting in a high PCE in DSSCs.

3.2 Structural and electronic properties of the dye-adsorbed TiO_2 system

3.2.1 Structural properties. Anatase TiO_2 (101) surface is known as the most stable and prominent semiconductor that is widely used in DSSCs. The DFTB optimized structure of $(TiO_2)_{256}$ system is shown in Fig S1 in the Supporting Information. The outmost atoms of TiO_2 anatase (101) surface are displayed in Fig. 3(a). In this

investigation, the possible adsorption configurations of BA group for C258 bonded to TiO_2 based on the structure parameters mentioned above are represented schematically in Fig. 3(b) where the used abbreviations Mha and BBH follow previous theoretical and experimental work.[22, 61-64] (The complete different adsorption modes of C258 on the surface of TiO_2 are provided in Fig. S2.) Values of the adsorption energies for both Mha and BBH are summarized in Table 1, together with a few key structural parameters (Ti-O lengths and O1-C-O2 angle). In Mha configuration, an O atom of BA bonds to Ti_{5c} with a bond length of 1.97 Å, and this adsorption mode also provides one strong hydrogen bonding between H atom and O_{2c} atom of TiO_2 surface, with an O_{2c}-H length of 1.40 Å. While in BBH configuration, the two oxygen atoms of BA interact with two titanium atoms on the TiO_2 (101) surface forming bidentate stucture, and the proton of benzoic acid transfers to the O_{2c} site near the adsorption site. The two Ti-O lengths and O_{2c}-H length are 2.12, 2.10, 1.08 Å, respectively, as shown in Fig. 3(b) and Table 1. Both Ti-O bond lengths are comparable to the Ti-O separations (1.93/1.97 Å) in bulk TiO_2, suggesting that there is strong chemisorption of C258 on the anatase (101) surface. The adsorption energies were calculated via Eq. (1) as mentioned before. In Table 1, the adsorption energy is 0.198 eV for Mha pattern and 0.845 eV for BBH, which indicates that the structure of BBH is more stable than Mha. Our result is consistent with previous findings for M1[23], M3[23], C2-1[24], NKX dyes[65], boric acid[66], and acetic acid[27] on TiO_2 anatase (101) surface where BBH is the more favorable choice , but in contrast to the cases of N749 dye[29] and formic acid[22] adsorbed on TiO_2 surface.

Interestingly, Tateyama et al. pointed out the formation of hydrogen bond between the proton in the carboxyl anchor and the surface O_{2c} site is responsible for the most stability of Mha mode for N749 dye on TiO_2 (101) surface.[29] The equivalent hydrogen bond is found in the Mha mode of C258 on TiO_2 (101) surface as well, see Figure 3, but it doesn't change the fact that the BBH mode is more stable than Mha. This clearly shows that the stability of varying adsorption modes of anchoring group is system dependent and deserves further studies to gain deeper understandings.

3.2.2 Electronic properties. The electronic band structure of $(TiO_2)_{256}$ (see Fig. S3.) shows that the direct band gaps at Γ point of TiO_2 in vacuum is 2.856 eV, which is very close to the experimental value of anatase bulk 3.2 eV, and much better than other theoretical calculations of 2.0 and 2.14 eV.[67-69] The density of states (DOS) of $(TiO_2)_{256}$ (see Fig. S4.) shows a broad, filled valence band (VB) and a broad, empty conduction band (CB), separated by a free band gap. The top of VB and bottom of CB are mainly of oxygen 2*p*-orbital and Ti 3*d*-orbital character, which is consistent with previous theoretical studies.[64, 70] Therefore, the DFTB method employed in this work is validated to provide reasonable and reliable calculation results. To explore the bonding interactions between C258 and the TiO_2 surface, we plotted the total density of states (TDOS)/ projected density of states (PDOS) for the clean and the adsorbed complexes presented in Fig. 4 and Fig. 5. The TDOS of TiO_2 contains broad valence and conduction bands separated by a wide band gap. After adsorption, the dyes introduce sharp occupied molecular bands in the band gap in both Mha and BBH systems. Compared to the bare TiO_2, the TDOS and PDOS of C258 adsorbed onto

TiO_2 point out a significant upward shift of the conduction band and the valence band edge of TiO_2. Regarding the difference between Mha and BBH, the latter shows a significantly upper CB edge shift than the former, which in turn agrees with the experimental observed trend to increase the open circuit potential (V_{oc}) of DSSCs.[71] At the same time, this highlights the importance of the dye anchoring mode for tuning the CB energy of TiO_2. In Fig. 4, it can be clearly seen that the DOS of the dye has a strong overlap with the valence band and the higher energy conduction band of the TiO_2 semiconductor over a wide range of energy, which means C258 introduces few π-occupied levels on the top of the TiO_2 valence band. The new π-occupied levels from the dye become the new top of the valence band for both Mha and BBH systems. However, the BBH pattern has a stronger overlap between C258 and the conduction bands and a more evident upper CB edge shift. The peak intensities of all dye/ TiO_2 systems on the edge of conduction band are higher and sharper than those of isolated TiO_2 system, indicating a strong electronic coupling between the LUMO of dye and the conduction band of TiO_2. Probably, these new π-occupied levels may account for a direct charge injection mechanism of a photoexcited electron transition from these π levels into the bottom of the conduction band in TiO_2. In the BBH system, as shown by Fig. 4, there is strong coupling over the C258-TiO_2 interface, and Fig. 5 shows that the LUMO of C258 is localized not only on the Ti (3*d*) orbital close to the adsorbate, but also mixes with different surface O 2*p*- and Ti 3*d*-orbitals. The Ti 3*d*-orbitals are split into a double $e_g(d_z^2$ and d_x^2-$_y^2$) and a triple $t_{2g}(d_{xz}, d_{yz}, d_{xy})$ orbitals. The e_g lies a higher energy than t_{2g}. Upon adsorption, the orbitals on C258 mix significantly with

the substrate e_g orbitals and the t_{2g} orbitals.

In Fig. 5, a sharp increased integral area of O-2*p* orbital in the valence band and a relatively small increased integral area of O-2*p* orbital in conduction band indicate the probability of electron injection into the TiO_2 surface when the dye adsorbed on it. The complete PDOS of all the orbitals are shown in Fig. S5 and Fig. S6. The HOMO of C258 in Mha is located near -0.4 eV, while the LUMO of C258 shifts towards the conduction band. The band gap of Mha system decreases with the strong couplings to 0.667 eV. In BBH system, the HOMO of C258 is located near 0 eV, and the LUMO of C258 in BBH system has a bigger shift towards the conduction band with increasing overlap than that in Mha system. The band gap of BBH system also decreases with the strong couplings to 0.228 eV. Comparing the PDOS of TiO_2 before and after adsorption in Fig. 5, the adsorption of C258 alters the electronic structure of the surface near the region of 2.5-4.5 eV, which is in the conduction band of the surface, indicating the adsorption of dye may favor the injection of the electron to the surface.

The TDOS and PDOS of both Mha and BBH adsorption modes have similar results. It's clear that the TDOS and PDOS strongly depend on the considered C258 adsorption mode. It is obvious that the band gap reduced from 2.856 eV to 0.667 and 0.228 eV for Mha and BBH modes, respectively. The band gap reduction of more than 2 eV is significantly related to the adsorbate contribution at the valence band maximum (VBM), which can be associated with the typical π^* orbital contributions of the isolated C258 molecule. The significant upshift of VBM is due to the transfer of protons in C258 to the surface. An upshift of the conduction band minimum (CBM)

appears for the dipole pointing out from the surface, which has been proved to play an important role in the experimentally measured increased V_{oc} values in some organic dyes.[33, 71] At the dye/ TiO_2 interface, the HOMO of C258 lies within the band gap of the semiconductor and the LUMO of C258 is at least 0.4 eV above the CB edge, and thus can provide a sufficient driving force for the electron injection into the semiconductor.

The band structures of the two binding patterns are shown in Fig. 6. After adsorption, the new π-occupied levels correspond to each linear band structures. It is clear to see that the BBH system has more introduced levels in both valence and conduction bands. Comparing the two adsorption patterns the Fermi level shifts by about 0.8 eV from Mha system to BBH system. The obvious difference in the position of valence band and conduction band may account for the different electron injection strength for different binding modes.

3.2.3 Electron injection mechanism. About the electron injection mechanism from C258 to TiO_2 system, we consider two possible characteristics. Firstly, the intermolecular electrons are excited to bring electrons towards the surface, increasing the overlap between the LUMOs of dye and TiO_2 surface, thus improving the electron injection. Secondly, the band gap can decrease by increasing the open circuit potential and make a red shift in the adsorption spectrum to improve the efficiency of light-harvesting. In the band structures shown in Fig. 6, the decrease of the band gap values between CBM and VBM at Γ point, especially in BBH system, makes it more favorable to inject the electron to the surface.

To get more insights into the electron injection mechanism of Mha and BBH systems, the band structure and partial orbital charge densities for the Γ point of VBM, VBM-1, VBM-2, VBM-3, CBM, CBM+1, CBM+2, CBM+4 bands are selected and displayed in Fig. 7 and Fig. 8, respectively. In Mha, as shown in Fig. 7, the electron densities from VBM, VBM-1, VBM-2 are primary located on the dye adsorbed on the surface of TiO_2, while the electron densities of CBM to CBM+4 are mainly located on the TiO_2 surface. The electron densities distributed in the VBMs and CBMs are mainly affected by the contribution of O-2*p* orbital and Ti-3*d* orbital as Fig. S5 depicted. Especially in the bands of CBM and CBM+1, the electron densities extend to the dye-TiO_2 interface, with small contribution of the adsorbate, which is corresponding to the effect of O-2*p* orbital to the conduction band in the region of 2.5-4.5 eV revealed by PDOS analysis as shown in Fig. 5, indicating the coupling between the dye excited state and the conduction band states of TiO_2. The partial orbital charge densities from the VBM to VBM-2 bands are mainly localized in the π conjugated orbitals of the dye, while part of the density of VBM-2 is on the adsorption interface, indicating a strong interaction between the dye and TiO_2. The density of VBM-3 band mainly distribute on the whole TiO_2 slab with a little density on the π conjugated groups of the dye, which is different from VBM-2 band. The partial orbital charge densities manifest that there are strong interactions between the dye C258 and TiO_2. This result indicates that the direct injection electron mechanism is possible.

In BBH system, as shown in Fig. 8, the electron densities from VBM, VBM-1 are

primary located on the adsorbed dye, and the density of VBM-2 is distributed on the adsorption interface, similar to the distribution of CBM+2, showing a strong interaction between the dye and TiO_2. While the electron density of VBM-3 is not distributed in the dye-TiO_2 interface, but spreads over the TiO_2 aloof the dye adsorption interface. The electron density for VBM-4 is found in the whole TiO_2 system. As to the CBMs, the electron densities of CBM to CBM+2 are mainly located on the interface. The densities in the band of CBM are distributed at the dye/ TiO_2 interface and the π conjugated groups of the dye, with a big contribution of the adsorbate, which is different from the CBM of Mha system. The CBMs' electron densities are significantly affected by the contribution of Ti-3*d* and O-2*p* orbitals as shown by Fig. S6. In BBH, the lowest unoccupied CB states are mainly localized on the TiO_2 surface with big contributions from the adsorbates. These unoccupied molecular orbitals are higher in energy and similar to those for the isolated (gas-phase) molecule as shown in Fig. S7. We refer to these as LUMO to LUMO+2. In DSSCs, these levels play a central role in heterogeneous electron transfer and their electronic coupling to the surface is therefore particularly attractive. The strength of the interfacial interaction influences the rate of electron injection from the excited dye into the TiO_2 surface. The adsorbate state with a strong coupling to the surface can be expected to possess an orbital that is delocalized over the surface as well as the benzene acid group. A weak coupling would show a concentration of the orbital contribution on the benzene ring. For our systems, there are strong couplings over the interface: the CBMs are delocalized over the adsorbate and the substrate slab, and not

localized only on the Ti-3*d* orbital close to the adsorbate. The LUMO π* system of C258 is conjugated almost over the whole molecule. The anchoring group contributions to the adsorbate part of the LUMOs are estimated from their PDOS contributions. As the band structure shown in Fig. 8, CBM+2 and CBM+1 in BBH are almost degenerate in energy and about 1 eV higher than CBM, so it is not surprising that the coupling between the dye and TiO_2 in CBM+2 and CBM+1 is much weaker than that in CBM, illustrating that the orbital matching in energy influences the interfacial electronic coupling significantly.

Fig. S7 combined with Fig. 7 and Fig. 8 shows that the frontier occupied molecular orbitals HOMO, HOMO-1, HOMO-2 of C258 just correspond to the partial orbital charge densities of VBM, VBM-1, VBM-2 bands, respectively. The LUMO of C258 shows that its electron delocalized in the π conjugated groups and acceptor parts. These frontier occupied orbitals are provided to make out the correlation with the molecular orbitals of the isolated dye C258. These relevances lead support to the direct injection mechanism that the electrons generated from the photo-excited C258 are probably injected into the conduction band of TiO_2 directly.

Efficient electron injection requires the electron injection is faster than the excited state decay of the dye. A strong electronic coupling between the dye and the semiconductor is favorable for higher electron injection efficiency. The electron injection efficiency also depends on other aspects,[72, 73] including the reorganization energy, the dye excited state oxidation potential, the semiconductor acceptor density of states, the ions in the electrolyte, the dye excited state lifetime, the dye

aggregations, which are not considered here.

4. Conclusions

DFT calculations on the structure and optical properties of C258 show that it has remarkable charge-transfer characteristics, which can induce fast electron injection from the excited dye to the conduction band of TiO_2. The structural and electronic properties of C258 sensitized TiO_2 system has been explored by using DFTB calculations. In view of the adsorption binding function of anchoring group with the TiO_2 surface, both monodentate (Mha) and bidentate bridging (BBH) modes have been considered. The dye's binding modes influence the shape of the lowest energy band with a variable spread depending on the adsorption modes considered. The calculated adsorption energy and interface couplings indicate that the BBH binding structure is favored over the Mha one. Visualized partial orbital charge densities demonstrate strong mixing of adsorbate orbitals with the substrate orbitals and reveal remarkable charge transfers in their photo-excitation processes for both systems. At the same time, the strong couplings are confirmed by a detailed analysis of the adsorbate contributions to the TDOS, PDOS and partial orbital charge densities. The adsorption of C258 reduces the band gap of TiO_2 to less than 1 eV, leading to the upshift of VBM and CBM, which is beneficial for the increase of V_{oc}. The predicted structural and electronic properties of the adsorption systems reveal that the direct electron injection, which turns up from the electrons photoexcited from the HOMOs orbitals of C258 to the conduction bands of TiO_2. This investigation provides a basis to further make out the interaction between the dye and the semiconductor as well as

the injection mechanism.

Acknowledgements

The authors gratefully acknowledge financial support from the Major State Basic Research Development Programs of China (2011CBA00701, 2012CB721003), the National Natural Science Foundation of China (21303007), the Specialized Research Fund for the Doctoral Program of Higher Education (20131101120053), the Excellent Young Scholars Research Fund of Beijing Institute of Technology (2013YR1917), and Beijing Key Laboratory for Chemical Power Source and Green Catalysis (2013CX02031). This work is also supported by the opening project of State Key Laboratory of Explosion Science and Technology (Beijing Institute of Technology). The opening project number is XXXXXXXX. ZDKT12-03

Appendix A. Supporting information

Electronic Supplementary Information (ESI) available: Optimized structures, band and DOS structure of $(TiO_2)_{256}$ and two adsorption systems, and the selected frontier molecular orbitals of C258. See DOI: 10.1039/b000000x/

References

1. B. Oregan and M. Grätzel, *Nature*, 1991, **353**, 737-740.
2. A. Hagfeldt and M. Grätzel, *Acc Chem Res*, 2000, **33**, 269-277.
3. M. K. Nazeeruddin, F. De Angelis, S. Fantacci, A. Selloni, G. Viscardi, P. Liska, S. Ito, B. Takeru and M. Grätzel, *J Am Chem Soc*, 2005, **127**, 16835-16847.
4. D. S. Zhang, T. Yoshida, T. Oekermann, K. Furuta and H. Minoura, *Adv Funct Mater*, 2006, **16**, 1228-1234.
5. P. Péchy, T. Renouard, S. M. Zakeeruddin, R. Humphry-Baker, P. Comte, P. Liska, L. Cevey, E. Costa, V. Shklover, L. Spiccia, G. B. Deacon, C. A. Bignozzi and M. Grätzel, *J Am Chem Soc*, 2001, **123**, 1613-1624.
6. M. Grätzel, *J Photochem Photobiol A*, 2004, **168**, 235-235.
7. A. Yella, H. W. Lee, H. N. Tsao, C. Y. Yi, A. K. Chandiran, M. K. Nazeeruddin, E. W. G. Diau, C. Y. Yeh, S. M. Zakeeruddin and M. Grätzel, *Science*, 2011, **334**, 629-634.
8. S.-L. Chen, L.-N. Yang and Z.-S. Li, *J Power Sources*, 2013, **223**, 86-93.
9. L. N. Yang, Z. Z. Sun, S. L. Chen and Z. S. Li, *Dyes Pigm*, 2013, **99**, 29-35.
10. M. Zhang, Y. L. Wang, M. F. Xu, W. T. Ma, R. Z. Li and P. Wang, *Energy Environ Sci*, 2013, **6**, 2944-2949.
11. J.-H. Luo, Q.-S. Li, L.-N. Yang, Z.-Z. Sun and Z.-S. Li, *RSC Adv*, 2014, **4**, 20200-20207.
12. S. Mathew, A. Yella, P. Gao, R. Humphry-Baker, B. F. E. Curchod, N. Ashari-Astani, I. Tavernelli, U. Rothlisberger, M. K. Nazeeruddin and M. Grätzel, *Nat Chem*, 2014, **6**, 242-247.
13. M. Zhang, J. Zhang, Y. Fan, L. Yang, Y. Wang, R. Li and P. Wang, *Energy Environ Sci*, 2013, **6**, 2939-2943.
14. J. Zhang, L. Yang, M. Zhang and P. Wang, *RSC Adv*, 2013, **3**, 6030-6035.
15. T. Kitamura, M. Ikeda, K. Shigaki, T. Inoue, N. A. Anderson, X. Ai, T. Q. Lian and S. Yanagida, *Chem Mater*, 2004, **16**, 1806-1812.
16. M. Velusamy, K. R. J. Thomas, J. T. Lin, Y. C. Hsu and K. C. Ho, *Org Lett*, 2005, **7**, 1899-1902.
17. D. P. Hagberg, T. Edvinsson, T. Marinado, G. Boschloo, A. Hagfeldt and L. C. Sun, *Chem Commun*, 2006, 2245-2247.
18. D. P. Hagberg, J.-H. Yum, H. Lee, F. De Angelis, T. Marinado, K. M. Karlsson, R. Humphry-Baker, L. Sun, A. Hagfeldt, M. Grätzel and M. K. Nazeeruddin, *J Am Chem Soc*, 2008, **130**, 6259-6266.
19. G. L. Zhang, H. Bala, Y. M. Cheng, D. Shi, X. J. Lv, Q. J. Yu and P. Wang, *Chem Commun*, 2009, 2198-2200.
20. W. J. Fan, D. Z. Tan and W. Q. Deng, *Phys Chem Chem Phys*, 2011, **13**, 16159-16167.
21. J. X. Liang, C. Zhu and Z. X. Cao, *Phys Chem Chem Phys*, 2013, **15**, 13844-13851.
22. A. Vittadini, A. Selloni, F. P. Rotzinger and M. Grätzel, *J Phys Chem B*, 2000, **104**, 1300-1306.
23. K. Srinivas, K. Yesudas, K. Bhanuprakash, V. J. Rao and L. Giribabu, *J Phys Chem C*, 2009, **113**, 20117-20126.
24. C. O'Rourke and D. R. Bowler, *J Phys Chem C*, 2010, **114**, 20240-20248.
25. K. L. Miller, J. L. Falconer and J. W. Medlin, *J Catal*, 2011, **278**, 321-328.
26. K. L. Miller, C. B. Musgrave, J. L. Falconer and J. W. Medlin, *J Phys Chem C*, 2011, **115**, 2738-2749.

27. D. C. Grinter, M. Nicotra and G. Thornton, *J Phys Chem C*, 2012, **116**, 11643-11651.
28. M. Chan, T. Carrington and S. Manzhos, *Phys Chem Chem Phys*, 2013, **15**, 10028-10034.
29. K. Sodeyama, M. Sumita, C. O'Rourke, U. Terranova, A. Isam, L. Y. Han, D. R. Bowler and Y. Tateyama, *J Phys Chem Lett*, 2012, **3**, 472-477.
30. R. Luschtinetz, S. Gemming and G. Seifert, *Eur Phys J Plus*, 2011, **126**, 1-13.
31. P. Raghunath and M. C. Lin, *J Phys Chem C*, 2008, **112**, 8276-8287.
32. F. Schiffmann, J. VandeVondele, J. Hutter, R. Wirz, A. Urakawa and A. Baiker, *J Phys Chem C*, 2010, **114**, 8398-8404.
33. F. Labat, I. Ciofini and C. Adamo, *J Mater Chem*, 2012, **22**, 12205-12211.
34. M.-G. Ju and W. Liang, *J Phys Chem C*, 2013, **117**, 14899-14911.
35. J. Zhang, H.-B. Li, J.-Z. Zhang, Y. Wu, Y. Geng, Q. Fu and Z.-M. Su, *J Mater Chem A*, 2013, **1**, 14000-14007.
36. C. Anselmi, E. Mosconi, M. Pastore, E. Ronca and F. De Angelis, *Phys Chem Chem Phys*, 2012, **14**, 15963-15974.
37. R. Dovesi, R. Orlando, A. Erba, C. M. Zicovich-Wilson, B. Civalleri, S. Casassa, L. Maschio, M. Ferrabone, M. De La Pierre, P. D'Arco, Y. Noël, M. Causà, M. Rérat and B. Kirtman, *Int J Quantum Chem*, 2014, 10.1002/qua.24658.
38. Y. Noel, M. De La Pierre, C. M. Zicovich-Wilson, R. Orlando and R. Dovesi, *Phys Chem Chem Phys*, 2014, **16**, 13390-13401.
39. F. d. r. Labat, I. Ciofini, H. P. Hratchian, M. J. Frisch, K. Raghavachari and C. Adamo, *J Phys Chem C*, 2011, **115**, 4297-4306.
40. T. Kruger, M. Elstner, P. Schiffels and T. Frauenheim, *J Chem Phys*, 2005, **122**, 114110.
41. K. W. Sattelmeyer, J. Tirado-Rives and W. L. Jorgensen, *J Phys Chem A*, 2006, **110**, 13551-13559.
42. M. F. Elstner, T.; McKelvey, J.; Siefert, G, *J Phys Chem A*, 2007, **111**, 5607-5608.
43. Q. S. Li, R. Q. Zhang, S. T. Lee, T. A. Niehaus and T. Frauenheim, *Appl Phys Lett*, 2007, **91**, 043106.
44. Q. S. Li, R. Q. Zhang, T. A. Niehaus, T. Frauenheim and S. T. Lee, *J Chem Theory Comput*, 2007, **3**, 1518-1526.
45. N. Otte, M. Scholten and W. Thiel, *J Phys Chem A*, 2007, **111**, 5751-5755.
46. Q. S. Li, R. Q. Zhang, S. T. Lee, T. A. Niehaus and T. Frauenheim, *J Chem Phys*, 2008, **128**, 244714.
47. Q. S. Li, R. Q. Zhang, S. T. Lee, T. A. Niehaus and T. Frauenheim, *Appl Phys Lett*, 2008, **92**, 053107.
48. G. Dolgonos, B. Aradi, N. H. Moreira and T. Frauenheim, *J Chem Theory Comput*, 2010, **6**, 266-278.
49. S. Wangmo, R. Song, L. Wang, W. Jin, D. Ding, Z. Wang and R.-Q. Zhang, *J Mater Chem*, 2012, **22**, 23380-23386.
50. H. B. S. G. M. T. M. J. Frisch, G. E. Scuseria, M. A. Robb, J. R. Cheeseman, G. Scalmani, V. Barone, B. Mennucci, G. A. Petersson, H. Nakatsuji, M. Caricato, X. Li, H. P. Hratchian, A. F. Izmaylov, J. Bloino, G. Zheng, J. L. Sonnenberg, M. Hada, M. Ehara, K. Toyota, R. Fukuda, J. Hasegawa, M. Ishida, T. Nakajima, Y. Honda, O. Kitao, H. Nakai, T. Vreven, J. A. Montgomery, Jr., J. E. Peralta, F. Ogliaro, M. Bearpark, J. J. Heyd, E. Brothers, K. N. Kudin, V. N. Staroverov, R. Kobayashi, J. Normand, K. Raghavachari, A. Rendell, J. C. Burant, S. S. Iyengar, J. Tomasi, M.

Cossi, N. Rega, J. M. Millam, M. Klene, J. E. Knox, J. B. Cross, V. Bakken, C. Adamo, J. Jaramillo, R. Gomperts, R. E. Stratmann, O. Yazyev, A. J. Austin, R. Cammi, C. Pomelli, J. W. Ochterski, R. L. Martin, K. Morokuma, V. G. Zakrzewski, G. A. Voth, P. Salvador, J. J. Dannenberg, S. Dapprich, A. D. Daniels, O . Farkas, J. B. Foresman, J. V. Ortiz, J. Cioslowski and D. J. Fox, *Gaussian09*, Wallingford.

51. D. Chattopadhyay, S. Lastella, S. Kim and F. Papadimitrakopoulos, *J Am Chem Soc*, 2002, **124**, 728-729.
52. B. J. Lynch, P. L. Fast, M. Harris and D. G. Truhlar, *J Phys Chem A*, 2000, **104**, 4811-4815.
53. M. Cossi, N. Rega, G. Scalmani and V. Barone, *J Comput Chem*, 2003, **24**, 669-681.
54. A. Vittadini, A. Selloni, F. P. Rotzinger and M. Grätzel, *Phys Rev Lett*, 1998, **81**, 2954-2957.
55. Y.-F. Li, Z.-P. Liu, L. Liu and W. Gao, *J Am Chem Soc*, 2010, **132**, 13008-13015.
56. B. Aradi, B. Hourahine and T. Frauenheim, *J Phys Chem A*, 2007, **111**, 5678-5684.
57. M. Elstner, D. Porezag, G. Jungnickel, J. Elsner, M. Haugk, T. Frauenheim, S. Suhai and G. Seifert, *Phys Rev B*, 1998, **58**, 7260-7268.
58. G. S. Zheng, H. A. Witek, P. Bobadova-Parvanova, S. Irle, D. G. Musaev, R. Prabhakar and K. Morokuma, *J Chem Theory Comput*, 2007, **3**, 1349-1367.
59. H. Kusama, H. Orita and H. Sugihara, *Langmuir*, 2008, **24**, 4411-4419.
60. D. P. Hagberg, T. Marinado, K. M. Karlsson, K. Nonomura, P. Qin, G. Boschloo, T. Brinck, A. Hagfeldt and L. Sun, *J Org Chem*, 2007, **72**, 9550-9556.
61. M. R. Hoffmann, S. T. Martin, W. Y. Choi and D. W. Bahnemann, *Chem Rev*, 1995, **95**, 69-96.
62. T. Lana-Villarreal, A. Rodes, J. M. Pérez and R. Gómez, *J Am Chem Soc*, 2005, **127**, 12601-12611.
63. M. Nilsing, S. Lunell, P. Persson and L. Ojamae, *Surf Sci*, 2005, **582**, 49-60.
64. M. Nilsing, P. Persson and L. Ojamae, *Chem Phys Lett*, 2005, **415**, 375-380.
65. M. K. Nazeeruddin, R. Humphry-Baker, P. Liska and M. Grätzel, *J Phys Chem B*, 2003, **107**, 8981-8987.
66. K. Hara, T. Sato, R. Katoh, A. Furube, T. Yoshihara, M. Murai, M. Kurashige, S. Ito, A. Shinpo, S. Suga and H. Arakawa, *Adv Funct Mater*, 2005, **15**, 246-252.
67. R. Asahi, Y. Taga, W. Mannstadt and A. J. Freeman, *Phys Rev B*, 2000, **61**, 7459-7465.
68. H. Kusama, Y. Konishi, H. Sugihara and H. Arakawa, *Sol Energ Mater Sol C*, 2003, **80**, 167-179.
69. Z. Lin, A. Orlov, R. M. Lambert and M. C. Payne, *J Phys Chem B*, 2005, **109**, 20948-20952.
70. N. Santhanamoorthi, K. H. Lai, F. Taufany and J. C. Jiang, *J Power Sources*, 2013, **242**, 464-471.
71. P. Chen, J. H. Yum, F. De Angelis, E. Mosconi, S. Fantacci, S. J. Moon, R. H. Baker, J. Ko, M. K. Nazeeruddin and M. Gratzel, *Nano Lett*, 2009, **9**, 2487-2492.
72. R. Katoh, A. Furube, A. V. Barzykin, H. Arakawa and M. Tachiya, *Coordin Chem Rev*, 2004, **248**, 1195-1213.
73. A. Listorti, B. O'Regan and J. R. Durrant, *Chem Mater*, 2011, **23**, 3381-3399.

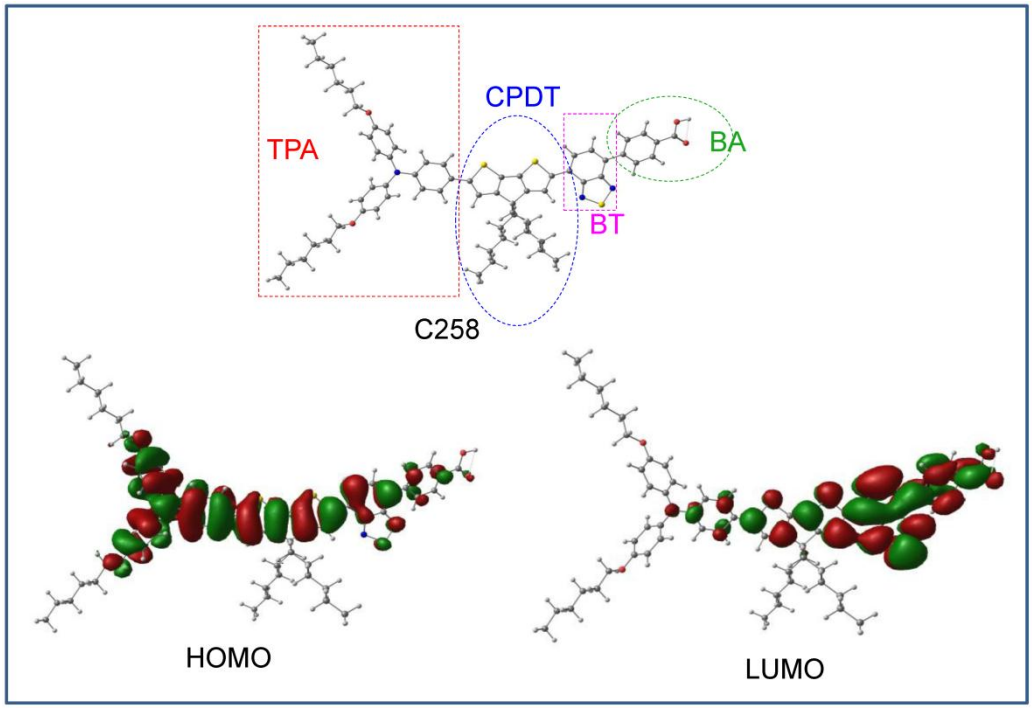

Fig. 1 Optimized geometry and the HOMO and LUMO molecular orbitals (isovalue is 0.01 au) on ground state of C258 (C: grey; H: white; O: red; S: yellow; N: blue).

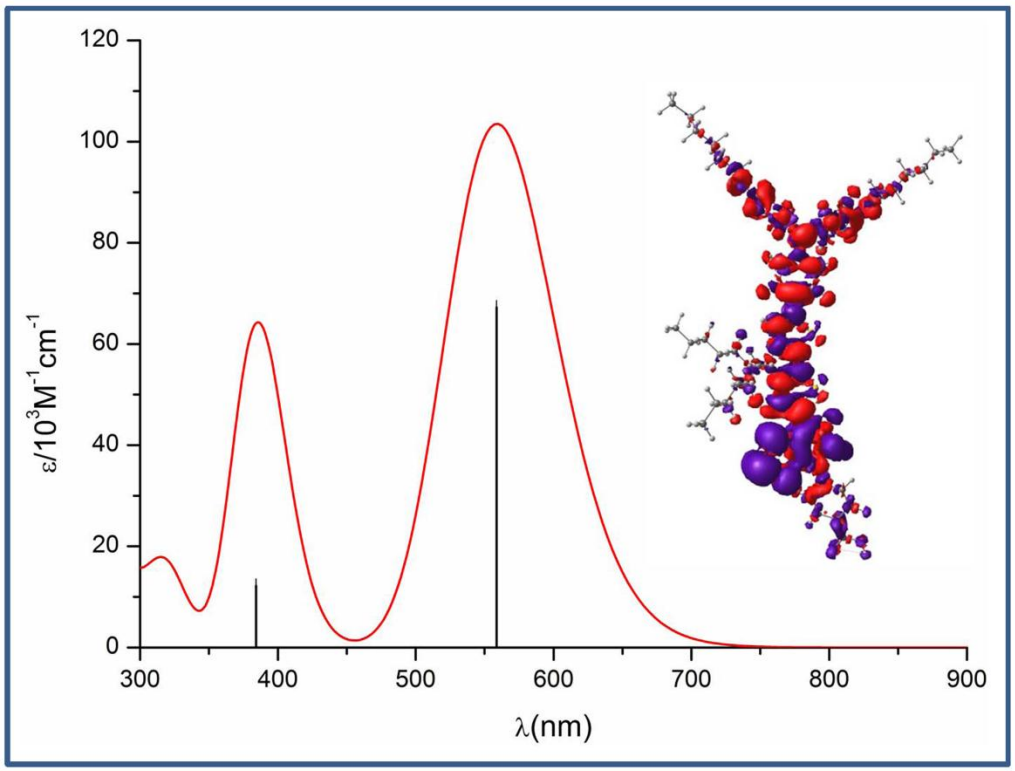

Fig. 2 Calculated absorption spectra by MPW1K/6-31G(d) for C258, along with the computed electron density difference between the first excited and ground state (purple and red refer to an increase and a decrease of electronic density, respectively; isovalue 0.0004 au).

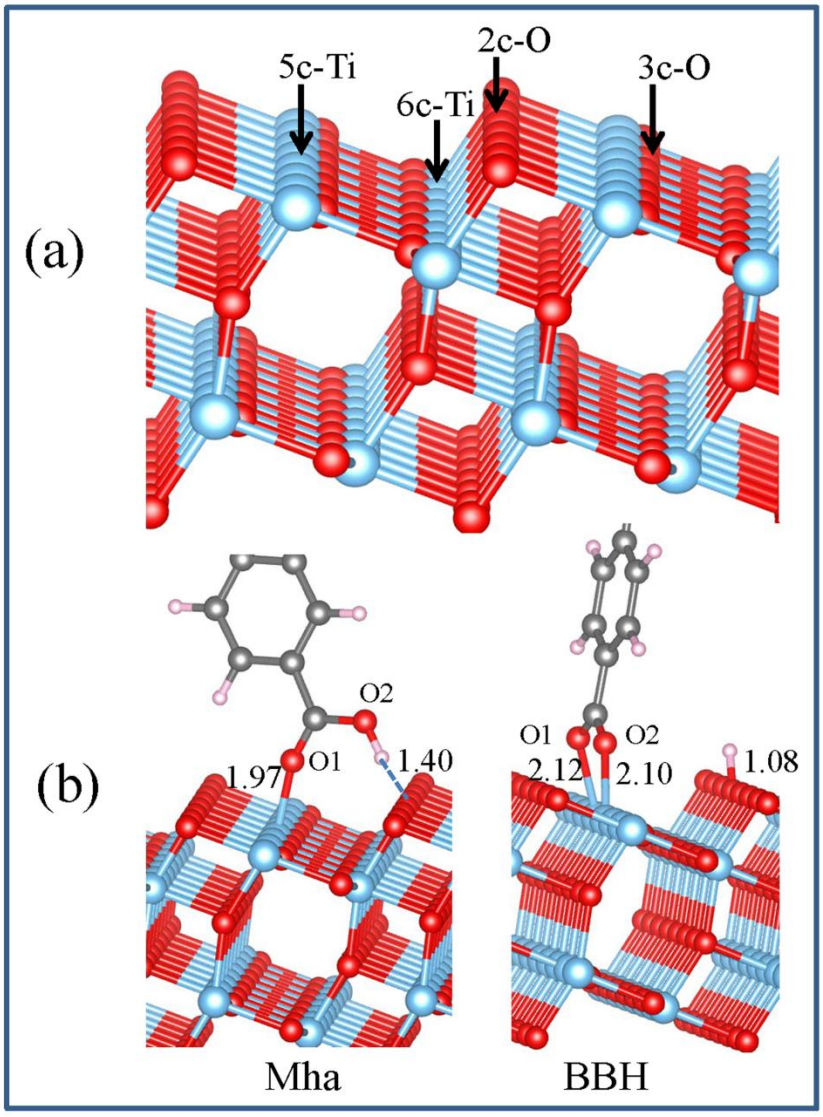

Fig. 3 (a) The clean TiO2 (101) surface. Different types of titanium and oxygen atoms on the TiO2 (101) surface are marked in red and light grey, respectively. The dimensions of surface cell used in the calculations are indicated by the arrows. (b) Two adsorption configurations (Mha and BBH) and selected key bond lengths (in angstrom) for C258 bonded to anatase (101) surface.

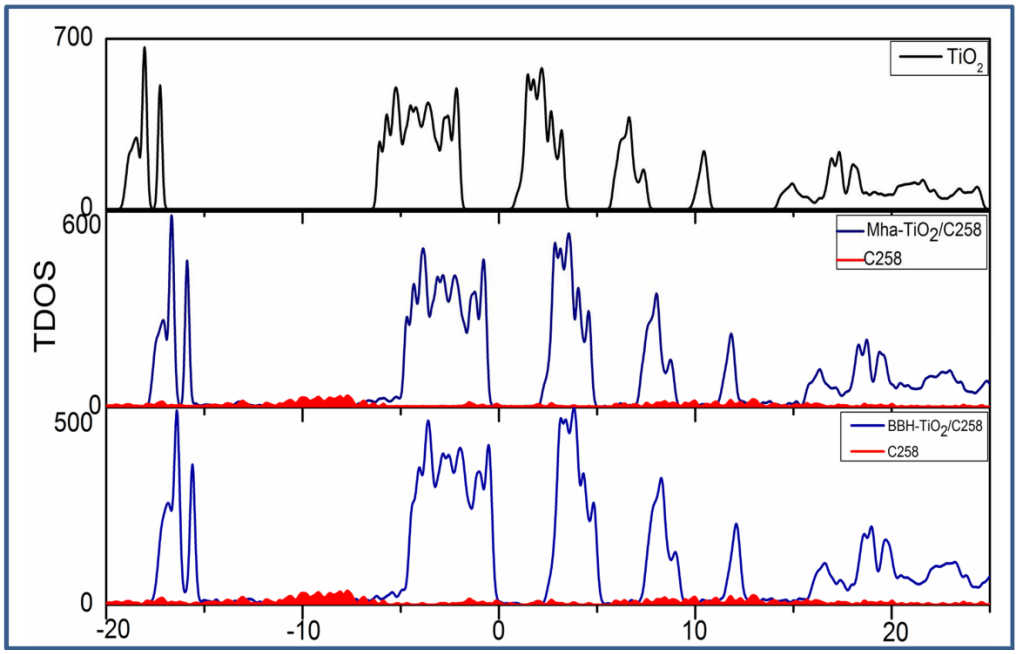

Fig. 4 Total DOS of TiO_2 (101) surface before and after C258 adsorption in Mha and BBH modes. The red integral area represents the DOS of the dye.

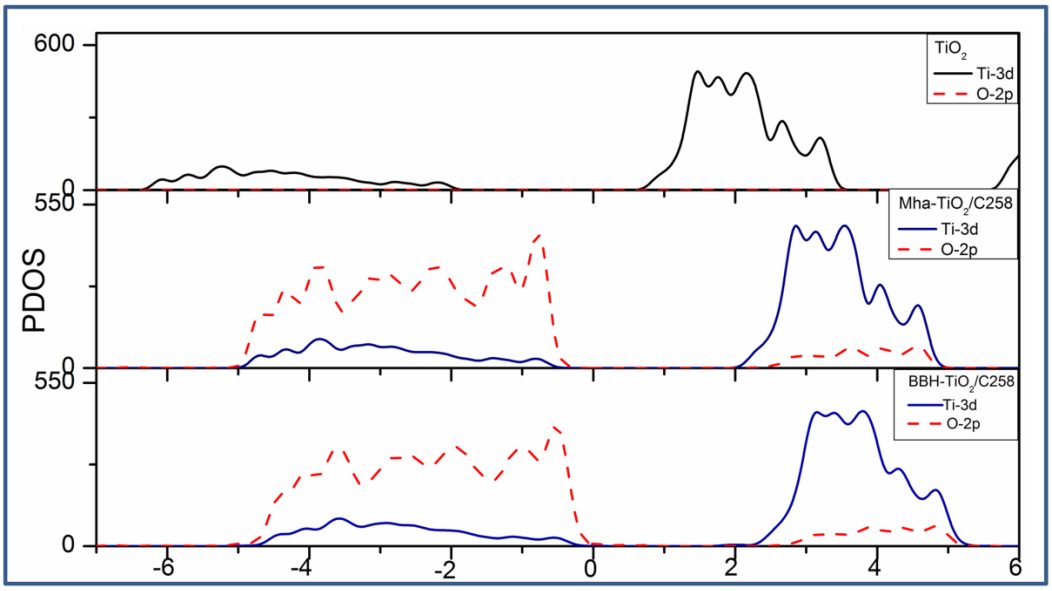

Fig. 5 PDOS of TiO_2 before and after C258 adsorption in Mha and BBH patterns. Black, blue lines and red dashed line represent Ti-3d and O-2p orbital, respectively.

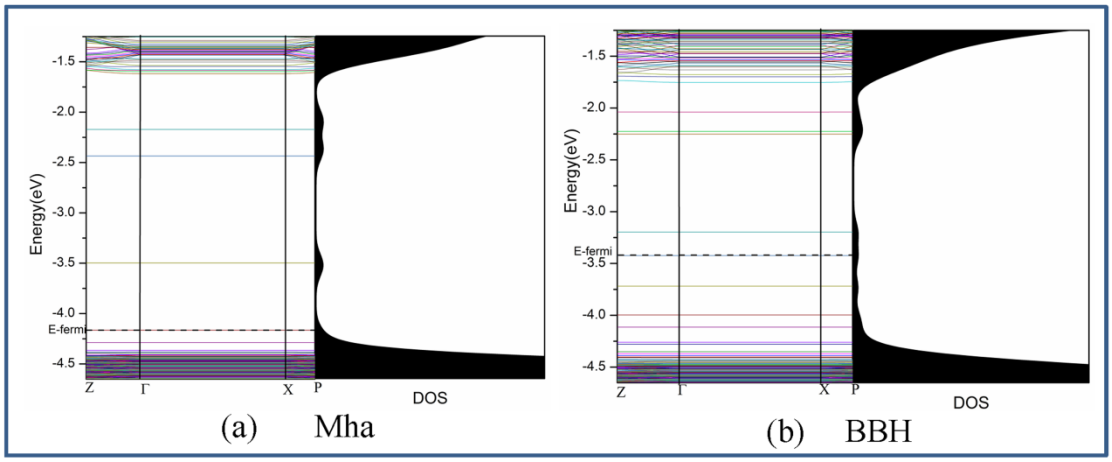

Fig. 6 Band stucture with density of states (DOS) of the C258 adsorbed TiO_2 system in (a) Mha and (b) BBH configuration.

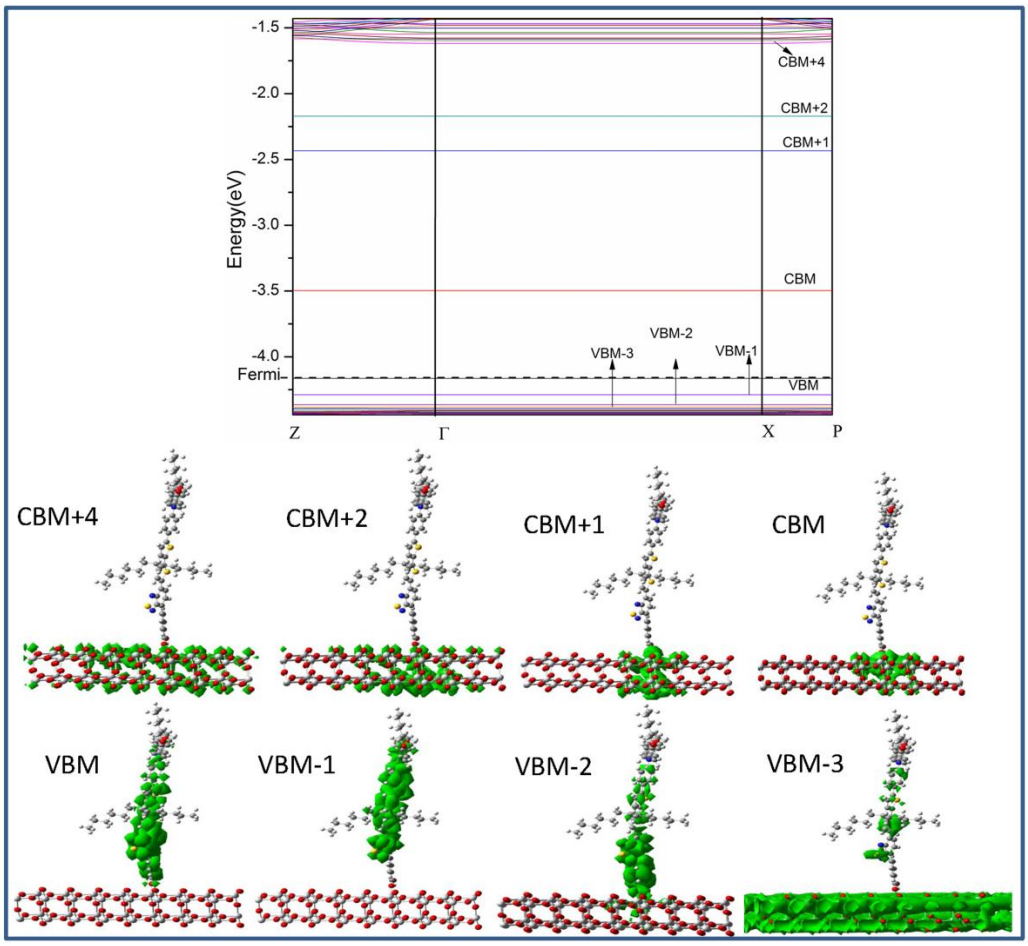

Fig. 7 Band structure of Mha system with partial orbital charge densities for the Γ point of some VBMs and CBMs bands corresponding to the relevant band structures.

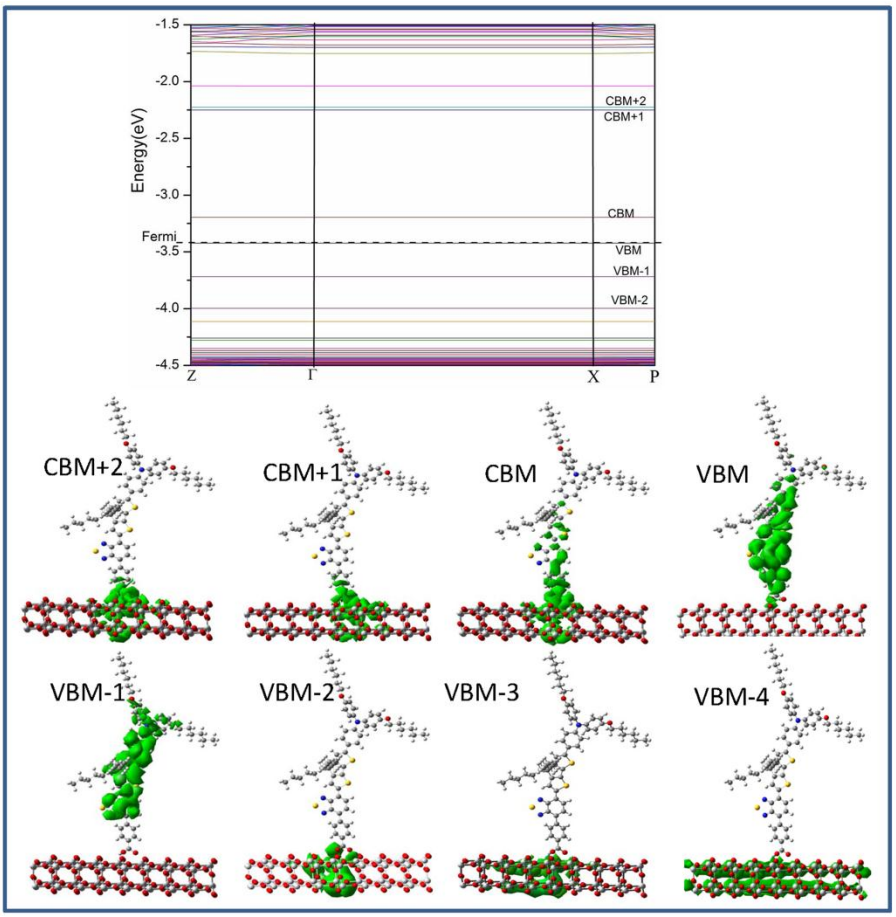

Fig. 8 Band structure of BBH system with partial orbital charge densities for the Γ point of some VBMs and CBMs bands corresponding to the relevant band structures.

Table 1 Adsorption energies (eV), bond lengths (Å), bond angels (deg), and Fermi energies (eV), band gap (eV) for two adsorption configurations of C258 on the anatase (101) surface. Atomic labelings are specified in Fig. 3(b).

Geometry	Ti-O1	Ti-O2	O_{2c}-H	O1-C-O2	E_{ads}	Band gap
TiO_2						2.856
TiO_2-101-C258-Mha	1.97	—	1.40	120	0.198	0.667
TiO_2-101-C258-BBH	2.12	2.10	1.08	120	0.845	0.228